THE JOURNAL OF PHYSICAL CHEMISTRY C

C: Energy Conversion and Storage; Energy and Charge Transport

High-Energy Charge-Separated States by Reductive Electron Transfer Followed by Electron Shift in Tetraphenylethylene – Aluminum(III) Porphyrin – Fullerene Triad

Niloofar Zarrabi, Christian Agatemor, Gary N. Lim, Adam J. Matula, Brandon J Bayard, Victor S. Batista, Francis D'Souza, and Prashanth K Poddutoori

J. Phys. Chem. C, **Just Accepted Manuscript** • DOI: 10.1021/acs.jpcc.8b09500 • Publication Date (Web): 06 Dec 2018

High-Energy Charge-Separated States by Reductive Electron Transfer Followed by Electron Shift in Tetraphenylethylene – Aluminum(III) Porphyrin – Fullerene Triad

Niloofar Zarrabi,[a] Christian Agatemor,[b] Gary N. Lim,[c] Adam J. Matula,[d] Brandon J. Bayard,[a] Victor S. Batista,[d] Francis D'Souza,*[c] Prashanth K. Poddutoori*[a]*

[a]Department of Chemistry & Biochemistry, University of Minnesota Duluth, 1039 University Drive, Duluth, MN, 55812, USA, Email: ppk@d.umn.edu. [b]Department of Biomedical Engineering, Johns Hopkins University School of Medicine, Baltimore, MD 21231 USA. [c]Department of Chemistry, University of North Texas, 1155 Union Circle, #305070, Denton, TX 76203-5017, USA, Email: francis.dsouza@unt.edu. [d]Department of Chemistry, Yale University, P.O. Box 208107, New Haven, Connecticut 06520-8107, USA, Email: victor.batista@yale.edu.

Abstract. A high potential supramolecular triad (TPE-AlPor←Im-C_{60}) composed of aluminum(III) porphyrin (AlPor), fullerene (C_{60}), and tetraphenylethylene (TPE) has been constructed. The fullerene and tetraphenylethylene units are bound axially to opposite faces of the porphyrin plane via coordination and covalent bonds, respectively. The ground and excited-state properties of the triad and reference dyads are studied using steady-state and time-resolved spectroscopic techniques. The transient data show that photoexcitation results in charge separation (CS) from tetraphenylethylene to the excited singlet state of the porphyrin (^{1}AlPor*), generating high-energy (2.14 eV) charge-separated state, $(TPE)^{\bullet+}$-$(AlPor)^{\bullet-}$ in toluene. A subsequent electron migration from the $AlPor^{-\bullet}$ to fullerene generates a second high-energy (1.78 eV) charge-separated state $(TPE)^{\bullet+}$-AlPor←Im-$(C_{60})^{\bullet-}$. The lifetime of the charge separation persists about 25 ns. The high energy stored in the form of charge-separated states along with its reasonable lifetimes makes these donor-acceptor systems potential electron-transporting catalysts to carry out energy-demanding photochemical reactions, especially in artificial photosynthesis for conversion of solar energy into chemical energy.

Introduction

One of the major challenges that mankind is facing at the present time is finding a clean and renewable energy source.[1-3] This is due to the nonrenewable nature of fossil fuel resources and their environmental problems. One promising way to address this is by developing artificial photosynthetic systems, which convert solar energy into chemical energy or electricity.[4-10] The design of artificial photosystems can be guided by the key steps of natural photosynthesis, such as the efficient capture of visible light, and the electron/hole separation through electron transfer process to give energy-rich charge separated state with longer lifetimes. One of the crucial components in photosynthesis is the reaction center complex, which generates a long-lived charge-separated state with sufficient energy to perform the water oxidation and CO_2 reduction reactions.[3, 11-13] The long-lived charge-separated state (CS) is achieved by a cascade of electron transfer processes through a variety of redox centers while the required high-energy to CS state is accomplished by integrating the photosystem I (PSI) and photosystem II (PSII) in a series, that is by Z-scheme design, where the PSI and PSII are operated by two different photons.

There has been a great progress in mimicking and modeling the various components of natural photosystem by using artificial Donor-Acceptor (D-A) systems. In this context, many elegant porphyrin based donor-acceptor systems have been reported in the literature.[14-18 15, 19-31] These reported model compounds not only revealed the intricate details of photoinduced energy and electron transfer processes but also provided design principles to achieve stable radical pairs with high efficiency and quantum yields by multistep electron transfer steps. One of the strategies was used in these donor-acceptor systems was to incorporate multiple electron donor units with redox gradient that is the later electron donor would have lower oxidation potential than the former electron donor.[32-35] Such a design principle ensures the sequential electron transfer processes. However, relatively less attention has been paid towards design and construction of donor-acceptor systems where high-energy charge-separated states can be produced in high quantum yields with sufficient lifetimes.[33, 36-38] In fact, the energy of the charge-separated state is as crucial as its lifetime because without enough potential energy it is not feasible to drive the catalytic processes in artificial photosynthetic systems, for example, water oxidation requires at least potential of 1.23 V. Therefore, there is a great deal for such donor-acceptor systems, and they could prove ideal candidates for solar energy conversion and storage applications. In this perspective, here we report new dyad (TPE-AlPor) and triad (TPE-AlPor←Im-C_{60}), using aluminum(III) porphyrin (AlPor) in combination with tetraphenylethylene (TPE) and fullerene (C_{60}). Similar to most of the other model compounds, we have chosen porphyrin as a photosensitizer because it absorbs strongly in the visible region, is often highly fluorescent, and not only have rich redox chemistry but also their optical and redox properties are easily tunable. Among porphyrins, aluminum (III) porphyrins (AlPor) are unique due to the following characteristic: (i) they form axial covalent bonds with alcohols, and carboxylic acids to form a 5-coordinate metal center, (ii) as Lewis acid, they have a sixth coordination site available for binding Lewis bases, such as pyridine and imidazole, and (iii) they have moderate redox potentials which make them a primary donor and/or acceptor.[39-51] These properties make Al(III) porphyrin as an excellent candidate for preparation of 'axial-bonding' type multi-component D-A systems where the photoinduced processes (energy and electron transfer) are perpendicular to the porphyrin plane, a crucial factor that maximizes the spatial separation of the charges produced by the electron transfer.[46-48, 50-51] In addition, the π^* orbital of the porphyrin resides in the same region of space as the axial ligands, increasing the electronic coupling between the excited state of the porphyrin and the acceptor and result in promoting electron transfer. On the other hand, the TPE derivatives have been selected as a primary electron donor. Due to its moderate oxidation potentials as well as its first oxidation potential is close to that of the AlPor, it is expected to generate high-energy charge separated state if it is coupled with AlPor through reductive electron transfer process. Also, the ether linkage was chosen between AlPor and TPE, which keeps the two redox components in close proximity, which may eventually help to increase the orbital overlap to promote the anticipated electron transfer. To stabilize the first radical pair, a well-known secondary electron acceptor fullerene (C_{60}) was chosen.[52-54]

Initially, the axial bonding ability of AlPor was exploited to construct the dyad AlPor-TPE. Later, the Lewis acid-base interactions, between Al center of the AlPor and N atom of the imidazole of C_{60}-Im, were employed to construct the triad molecule, TPE-AlPor←Im-C_{60}. The newly designed and synthesized compounds have been fully characterized by steady-state spectroscopic techniques, and their optical properties have been investigated using transient spectroscopic methods. We have also used density functional theory (DFT) calculations to elucidate and model the observed properties. Time-resolved studies have shown that these compounds undergo photoinduced electron transfer processes. In the TPE-AlPor dyad, AlPor serves as an electron acceptor to the TPE. In the case of triad TPE-AlPor←Im-C_{60}, initially, electron transfer occurs from TPE to AlPor followed by electron migration to C_{60}, which ultimately results $(TPE)^{\bullet+}$-AlPor←Im-$(C_{60})^{\bullet-}$. We will show that the charge-separated states, $AlPor^{-\bullet}$-$TPE^{+\bullet}$ and $(TPE)^{\bullet+}$-AlPor←Im-$(C_{60})^{\bullet-}$, have high energies as well as the stabilization of former charge-separated state by the secondary electron acceptor (C_{60}).

Experimental Section.

Synthesis. All the chemicals and solvents were obtained from Sigma-Aldrich, VWR or Fisher Chemicals and were used as received. Chromatographic materials were procured from Sigma-Aldrich or SiliCycle Inc. Synthesis of the precursor porphyrins such as 5,10,15,20-tetraphenylporphyrin (H_2Por), and its Al(III) derivative 5,10,15,20-tetraphenylporphyrinatoaluminum(III) hydroxide (AlPor-OH), were synthesized according to the literature procedures.[49-50] The synthesis details of the dyad TPE-AlPor and its reference compound AlPor-Ph are given below, Scheme 1. The Lewis acid-base interactions were employed to construct the dyad Ph-AlPor←Im-C_{60} and its corresponding supramolecular triad TPE-AlPor←Im-C_{60}, Scheme 2a. Synthesis of precursor compounds, TPE-OH and C_{60}-Im, are reported elsewhere.[32, 55]

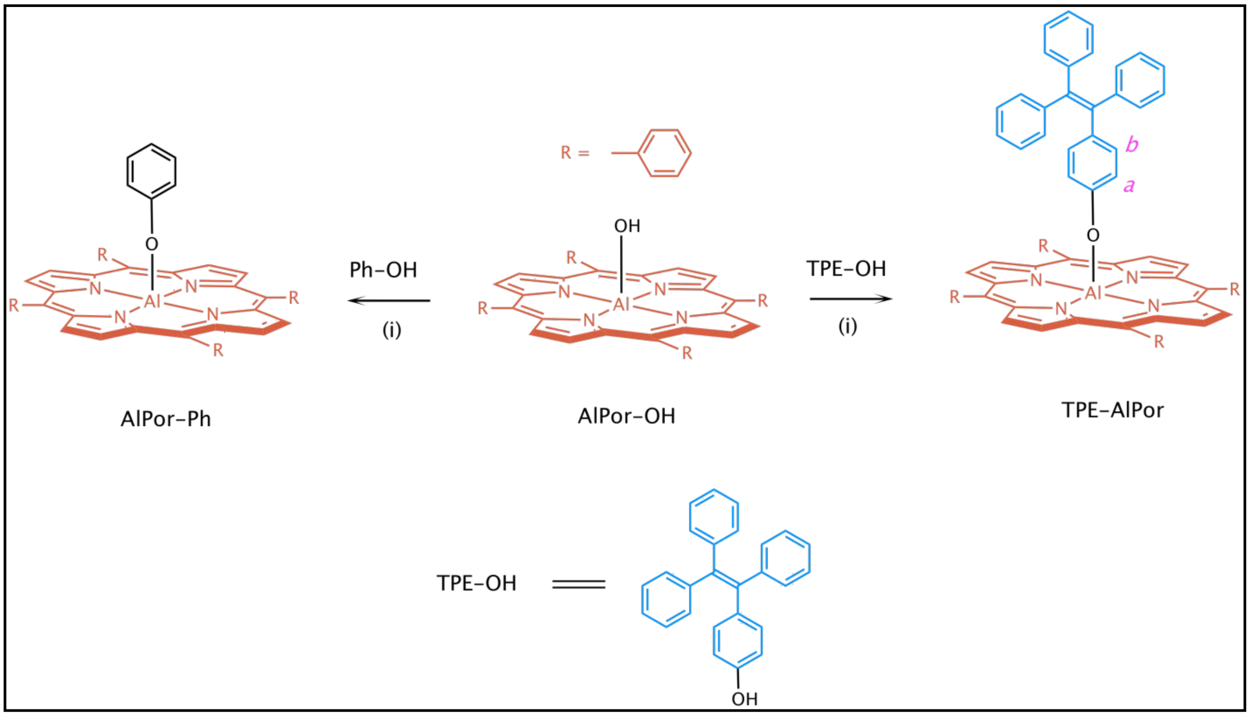

Scheme 1. Synthesis of the dyad TPE-AlPor and reference compound AlPor-Ph. Reaction conditions: (i) reflux in dry toluene for 12 h under N_2.

Preparation of TPE-AlPor. A mixture of AlPor-OH (100 mg, 0.152 mmol) and TPE-OH (54 mg, 0.152 mmol) in 30 mL of dry toluene was refluxed for 12 h under nitrogen atmosphere. The solvent was evaporated and the obtained solid was dissolved in dichloromethane. The resulting solution was dried over anhydrous Na_2SO_4 and evaporated to dryness. The solid was washed with boiling hexane to get the desired product in a pure form. Yield: 138 mg (92%). ESI MS: m/z 986.3091 for $[M]^+$, calculated 986.3560 for $C_{70}H_{47}AlN_4O$; 639.1785 for $[M – (O\text{-}TPE)]^+$. ^1H NMR ($CDCl_3$): δ, *ppm* 9.02 (s, 8H), 8.13 (d, 8H, J = 7.3 Hz), 7.76 (m, 12H), 7.09 (m, 2H), 7.02 (m, 2H), 6.96 (m, 4H), 6.76 (m, 2H), 6.63 (m, 3H), 6.47 (m, 2H), 5.48 (d, 2H, J = 9.0 Hz), 2.24 (d, 2H, J = 9.0 Hz).

Preparation of AlPor-Ph. A solution of AlPor-OH (100 mg, 0.152 mmol) and phenol (15 mg, 0.152 mmol) were dissolved in 30 ml of dry toluene, the resulting solution was refluxed for 12 h under nitrogen atmosphere. The product was purified in a manner analogous to that described above for AlPor-TPE. Yield: 95 mg (85%). ESI MS: m/z 639.1789 for $[M – (O\text{-}Ph)]^+$. ^1H NMR ($CDCl_3$): δ, *ppm* 9.05 (s, 8H), 8.16 (d, 8H, J = 7.6 Hz), 7.78 (m, 12H), 5.83 (m, 3H), 2.44 (d, 2H, J = 6.5 Hz).

Methods.

NMR and mass spectroscopy. NMR spectra were recorded with Bruker Avance 300 MHz and Varian 500 MHz NMR spectrometer using $CDCl_3$ as the solvent. ESI mass spectra were recorded on a Bruker MicroTOF-III mass spectrometer.

Electrochemistry. Cyclic voltammetric experiments (dichloromethane, 0.1 M tetrabutylammonium perchlorate (TBAP)) were performed on a BASi Epsilon electrochemical analyzer (working electrode: platinum, auxiliary electrodes: Pt wire; reference electrode: Ag/AgCl). The Fc^+/Fc (Fc = ferrocene, $E_{1/2}(Fc^+/Fc)$ = 0.48 V *vs* SCE in CH_2Cl_2, 0.1 M TBAP under our experimental conditions) redox couple was used to calibrate the potentials.

Steady-state spectroscopy: The UV/Vis spectra were recorded with an Agilent Cary 100 UV-VIS spectrometer. The concentration of the samples used for these measurements ranged from 1×10^{-6} M (porphyrin Soret band) to 5×10^{-5} M (Q-bands) solutions. Steady-state fluorescence spectra were recorded using a Photon Technologies International Quanta Master 8075-11 spectrofluorimeter, equipped with a 75 W xenon lamp, running with FelixGX software.

Titrations. Absorption titrations were carried out in dry *o*-dichlorobenzene (*o*-DCB) at concentration of 4.0×10^{-6} M appropriate for measuring the porphyrin Soret band. A solution containing the donor (D = TPE-AlPor or AlPor-Ph) was placed in a cuvette and titrated by adding aliquots of a concentrated solution of the acceptor (A = C_{60}-Im or 1-methylimidazole (Me-Im)). The acceptor solution also contained the donor at its initial concentration so that the porphyrin concentration remained constant throughout the titration. The binding constants were calculated using the Benesi-Hildebrand equation,[56] $[D]/Abs = (1/[A])(1/\varepsilon K) + (1/\varepsilon)$, where, [D] is the total concentration of bound and unbound donor and is kept fixed, Abs is the absorption of complex at the wavelength λ, [A] is the total concentration of the acceptor which is varied, K is binding constant and ε is the molar absorptivity of D-A complex. In an analogous manner, steady-state fluorescence titrations were carried out in dry *o*-DCB using solutions at constant concentration of D and varying concentration of A. The solutions were excited at the isosbestic point wavelength, which was obtained from the corresponding absorption titrations.

Calculations. Density function theory (DFT) was used to optimize the structures at the B3LYP[57]/def2SVP[58] level of theory. Frequency calculations were performed to verify that the obtained minimum geometry was stable. Single point energy calculations of the minimum structures in an implicit dichloromethane polarizable continuum model[59] were performed to determine solvated orbital energies. These calculations were used as part of a thermodynamic cycle to calculate redox potentials for the structures according to a previously established method.[60] Linear-response time-dependent DFT calculations[61] were performed with the CAM-B3LYP[62] to obtain the thirty lowest-energy singlet electronic transitions for the molecules. All calculations were performed using the Gaussian09 software package.[63] Orbital isosurfaces are shown with an isovalue of 0.02. Natural Transition Orbital (NTO) analysis[64] was used to visualize the calculated electronic transitions using a single pair of orbitals, from an excited 'particle' to an empty 'hole'.

Femtosecond laser flash photolysis. Femtosecond transient absorption spectroscopy experiments were performed using an Ultrafast Femtosecond Laser Source (Libra) by Coherent incorporating diode-pumped, mode locked Ti:Sapphire laser (Vitesse) and diode-pumped intra cavity doubled Nd:YLF laser (Evolution) to generate a compressed laser output of 1.45 W. For optical detection, a Helios transient absorption spectrometer coupled with femtosecond harmonics generator both provided by Ultrafast Systems LLC was used. The source for the pump and probe pulses were derived from the fundamental output of Libra (Compressed output 1.45 W, pulse width 100 fs) at a repetition rate of 1 kHz. 95 % of the fundamental output of the laser was introduced into a TOPAS-Prime-OPA system with 290 - 2600 nm tuning range from Altos Photonics Inc., (Bozeman, MT), while the rest of the output was used for generation of white light continuum. In the present study, the second harmonic 400 nm excitation pump was used in all the experiments. Kinetic traces at appropriate wavelengths were assembled from the time-resolved spectral data. Data analysis was performed using Surface Xplorer software supplied by Ultrafast Systems. All measurements were conducted in degassed solutions at 298 K.

Results and Discussions

Synthesis and Characterization. The synthesis and construction of dyads and triad are shown in Scheme 1 and Scheme 2. Aluminum(III) porphyrins are well known to form two axial bonds: (i) an axial Al-O bond through condensation with alcohols and (ii) an axial bond Al-X (X = N & O atom) through Lewis acid-base interactions.[46-51] These unique properties of aluminum(III) porphyrin were exploited to construct the investigated dyads (TPE-AlPor and Ph-AlPor←Im-C_{60}) and triad (TPE-AlPor←Im-C_{60}). Initially, the dyad TPE-AlPor was prepared by condensation of 5,10,15,20-tetraphenylporphyrinatoaluminum(III) hydroxide (AlPor-OH) with TPE-OH in quantitative yield (see Scheme 1). The Al center in the dyad, TPE-AlPor, acts as Lewis acid, therefore, Lewis base such as imidazole appended fullerene (C_{60}-Im) was employed to construct a supramolecular triad TPE-AlPor←Im-C_{60} (see Scheme 2a). A similar strategy was used to construct the dyad Ph-AlPor←Im-C_{60} starting from the reference compound AlPor-Ph (see Scheme 2b). The mass (ESI) spectra of dyad TPE-AlPor showed a low intensity peak ascribable to the parent M^+ ion, see Figure S1. However, the peaks due to those fragments obtained upon elimination of the axial ligand of TPE-AlPor and Ph-AlPor were found to be intense. The ^{1}H NMR spectra of dyad TPE-AlPor and unbound TPE-OH shown in Figure S2 and the data is summarized in the experimental section. As seen from Figure S2, the resonance positions of the protons *a* and *b* (see Scheme 1 for labels) on the bridging phenyl are quite different from those of corresponding protons in unbound TPE-OH. The ortho and meta (with respect to the hydroxy group) protons of the unbound TPE unit resonate at 6.57 and 6.90 ppm, respectively. The same protons in the dyad TPE-AlPor now resonate in upfield region that is at 2.25 and 5.48 ppm, respectively due to the ring current effect exerted by the aluminum(III) porphyrin. The ortho protons experience great shift because they are much closer to the porphyrin ring compare to the meta protons. Similar shielding effects were revealed on the remaining protons of TPE. However, their chemical shift depends on the distance between the proton and the porphyrin ring.

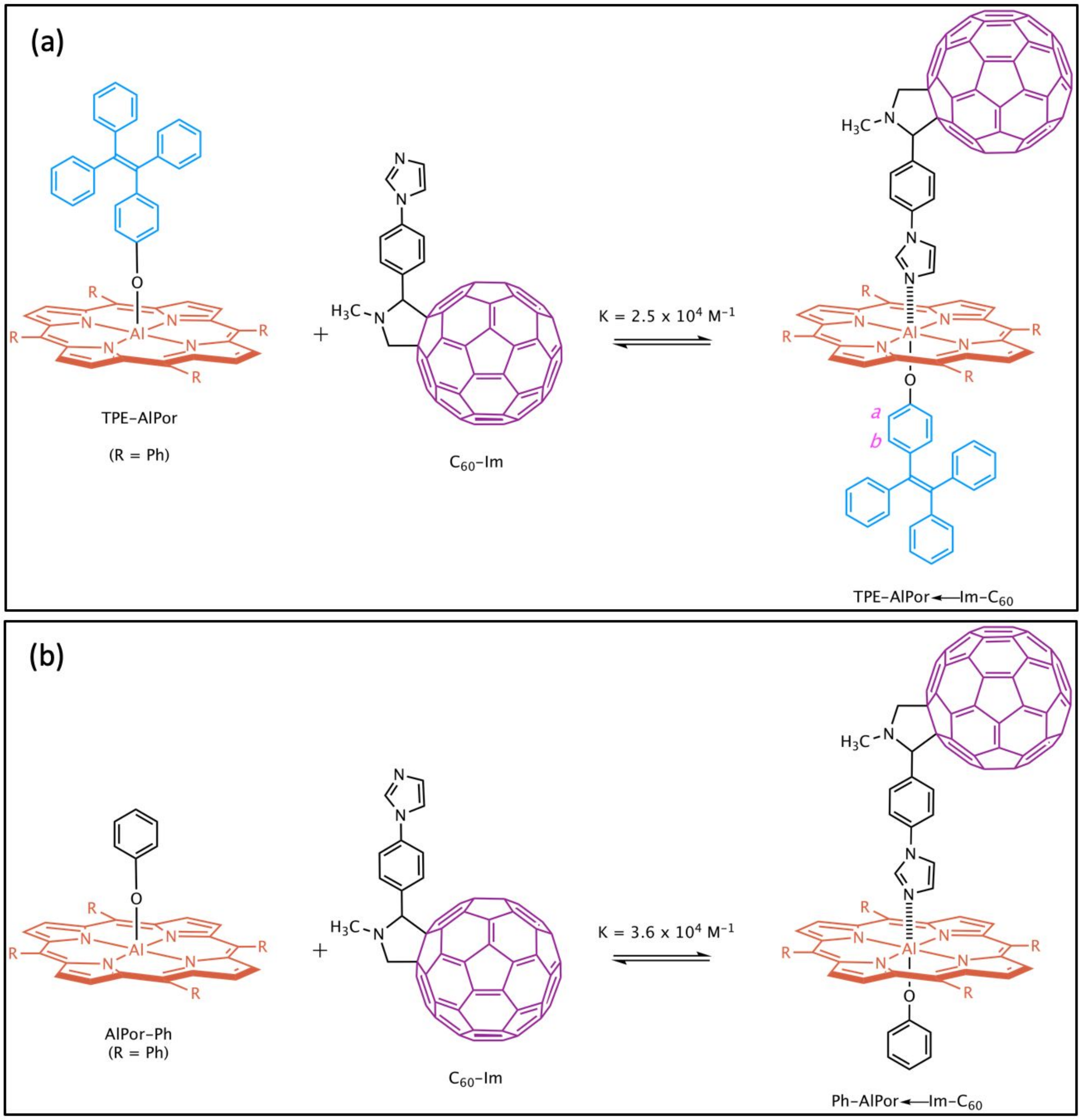

Scheme 2. The reaction schemes show the formation of (a) the triad TPE-AlPor←Im-C_{60} and (b) the dyad Ph-AlPor←Im-C_{60} in solution.

Figure S3 shows the ^{1}H NMR of 1:1 ratio of C_{60}-Im and TPE-AlPor (black) along with the individual spectra of TPE-AlPor (red) and C_{60}-Im (blue). In the coordination complex (see black spectrum), shielding due to the porphyrin ring causes an upfield shift of the C_{60}-Im protons on the imidazole unit, bridging phenyl group, and the five membered ring that is attached to the fullerene unit. The magnitude of the shift depends on the distance of the protons from the porphyrin ring, therefore the imidazole protons display the greatest shift indicating that coordination occurs via the imidazole group. These chemical shifts confirm the formation of supramolecular triad TPE-AlPor←Im-C_{60} in the solution. On the phenoxy bridging group, the protons a & b closest to the porphyrin ring show an increased upfield shift upon coordination (see Figure S3), suggesting that the aluminum(III) center lies out of the porphyrin plane in TPE-AlPor and is pulled into the plane when Im-C_{60} coordinates.

Absorption spectroscopy. The UV−visible spectra of the dyad TPE-AlPor and its reference compounds (AlPor-Ph and TPE-OH) were measured in dichloromethane, and the spectra are shown in Figure 1a. The band positions (Q-band and B- or Soret band) and their molar extinction coefficients (**ε**) are summarized in Table 1. The absorption spectrum of the dyad is essentially a linear combination of its reference porphyrins. Furthermore, the band positions and molar extinction coefficients (ε) of the dyad are similar to corresponding monomer porphyrins. Overall, the absorption studies suggest that there exist no or weak interactions between basal porphyrin (AlPor) and axial unit (TPE). The imidazole-appended acceptor, C_{60}-Im, has a broad absorption band in the ultraviolet region, Figure 1a.

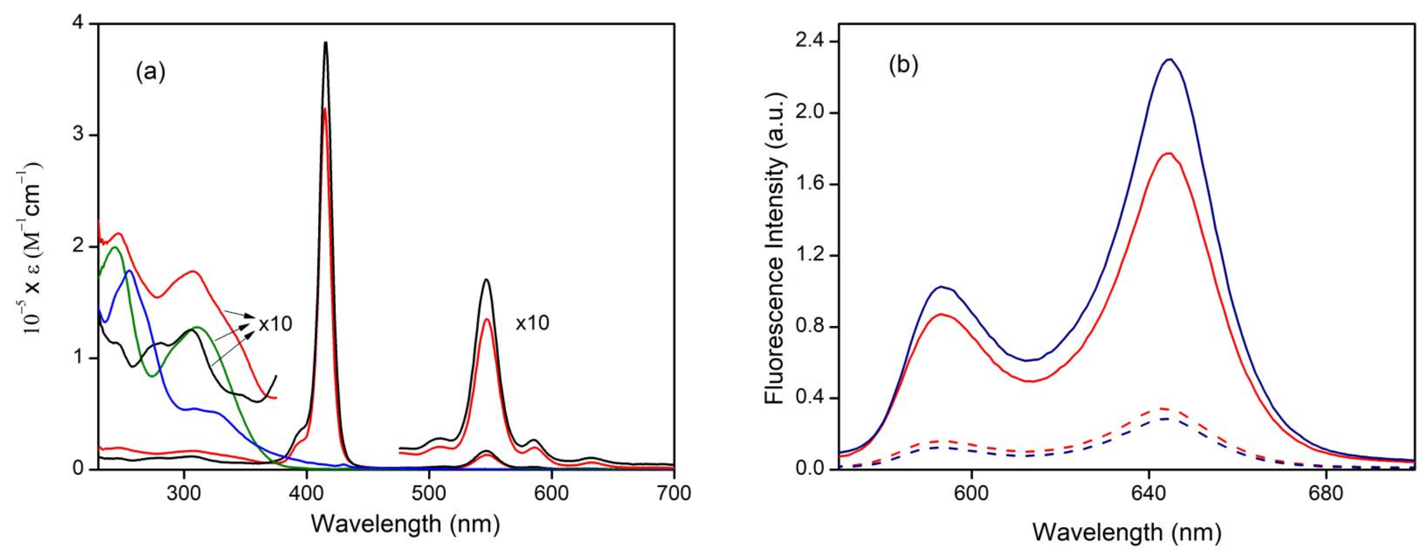

Figure 1. (a) UV−visible absorption spectra of TPE-AlPor (red) and its reference compounds AlPor-Ph (black), TPE-OH (green) and C_{60}-Im (blue) in dichloromethane. (b) Fluorescence spectra of TPE-AlPor (dashed line) and AlPor-Ph (solid line); red spectra in dichloromethane and blue spectra is toluene; excitation wavelength was 550 nm.

Table 1. UV-visible, fluorescence and redox data of investigated compounds in dichloromethane.

Sample	Potential [V *vs* SCE]		Absorption λ_{max} [nm] (log (ε [$M^{-1}cm^{-1}$]))			Fluorescence λ_{exc} = 550 nm
	Oxidation	Reduction	B-Band	Q-Band	Axial Ligand	λ_{max}, nm
TPE-AlPor	0.93, 1.17	−1.21, −1.61	415 (5.51)	509 (3.31), 547 (4.13), 586 (3.30)	309 (4.25)	593, 643
AlPor-Ph	0.95, 1.19	−1.21, −1.61	415 (5.58)	509 (3.45), 546 (4.23), 585 (3.42)	-	593, 645
C_{60}-Im[a]	-	−0.65, −1.03, −1.57	-	-	255 (5.25), 308 (4.73)	-
TPE-OH	1.13	-	-	-	310 (4.11)	-

[a]Measured in *o*-DCB, 0.1 M TBA.ClO_4[32]

To complement the triad TPE-AlPor←Im-C_{60} formation in a solution, absorption titrations were performed. Figure 2a shows the formation of the triad TPE-AlPor←Im-C_{60} in *o*-DCB and was monitored by absorption titrations. Upon addition of C_{60}-Im, the porphyrin B-band & Q-bands were shifted from 418, 546 and 588 nm to 422, 561 and 600 nm, respectively. An isosbestic points are observed at 422 and 555 nm, indicating the formation of TPE-AlPor←Im-C_{60}. The shifts in the porphyrin bands are typical of axial coordination of nitrogen ligands to AlPors. Benesi−Hildebrand analysis[56] (Figure 2a, inset) gives a linear plot indicating that a 1:1 complex is formed, and the slope yields a binding constant $K = 2.5 \times 10^4$ M^{-1}. Together with NMR and absorption titrations, formation of the triad TPE-AlPor←Im-C_{60} in solution was established. Similar absorption changes were observed from control titration experiments, i.e. TPE-AlPor with Me-Im (Figure S4, $K = 4.0 \times 10^4$ M^{-1}), AlPor-Ph with C_{60}-Im (Figure 2b, $K = 3.6 \times 10^4$ M^{-1}) and AlPor-Ph with Me-Im (Figure S5, $K = 4.5 \times 10^4$ M^{-1}).

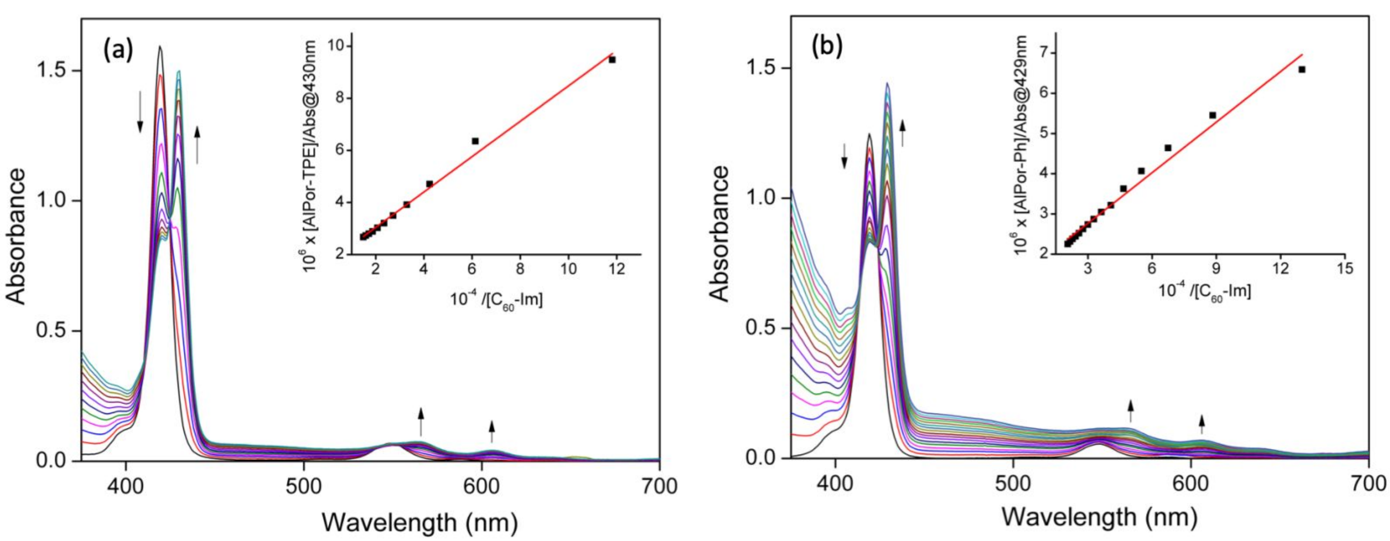

Figure 2. Absorption titrations of: (a) TPE-AlPor with C_{60}-Im. C_{60}-Im was added up to 6.7×10^{-5} M in 40 μL

(8.5×10^{-6} M) increments to 1 mL (4.0×10^{-6} M) solution of TPE-AlPor, the inset shows the Benesi-Hildebrand plot of the change of absorbance at 430 nm. (b) AlPor-Ph with C_{60}-Im. C_{60}-Im was added up to 9.7×10^{-5} M in 20 μL (7.8×10^{-6} M) increments to 1 mL (4.0×10^{-6} M) solution of AlPor-Ph, the inset shows the Benesi-Hildebrand plot of the change of absorbance at 429 nm. All titrations were performed in *o*-DCB.

Density functional theory. In order to obtain further insights into the electronic interactions between the components of the dyad and triad, density functional theory calculations were performed to optimize the relevant structures, characterize their frontier orbitals, and simulate UV-VIS spectra (details of computational procedures are found in the experimental section), see Figures 3 and 4. The calculated spectra shows strong agreement with the experimental results both in terms of peak positions and in the relative intensities between AlPor-Ph and TPE-AlPor. Of particular interest in this study is the transition at 550 nm, as this is the excitation wavelength used in the transient absorption studies. Natural Transition Orbital (NTO) analysis shows that in the TPE-AlPor molecule, this transition originates on the porphyrin core and the excited state is localized to the porphyrin core as well (Figure S6). This helps explain why such small differences are observed in the UV-VIS spectra between AlPor-Ph and TPE-AlPor, despite the strong electron-donating effects of TPE. Examining the frontier orbitals of TPE-AlPor shows that the HOMO is localized to the TPE group, which is to be expected given the nature of the TPE adduct. Moreover, a close inspection reveals that the HOMO of the TPE is predominantly localized on the bridging phenyl group. The HOMO-1, LUMO, and LUMO+1 are all localized to the porphyrin ring and are primary contributors to the transition at 550 nm. Examining the frontier orbitals of the triad structures shows that the HOMO and HOMO-1 of both the dyad and triad are qualitatively similar, giving further indication to the extent of electronic decoupling between the C_{60} portion of the triad and the TPE portion of the triad as seen in Figure 4. The DFT calculations also give insights into the structures. The radius of TPE, AlPor, and C_{60} are found to be about 6.2, 8.8 and 3.6 Å while the center-to-center distances in the dyads TPE-AlPor and Ph-AlPor←Im-C_{60} and the triad TPE-AlPor←Im-C_{60} are estimated to 7.5, 15.5 and 22 Å, respectively.

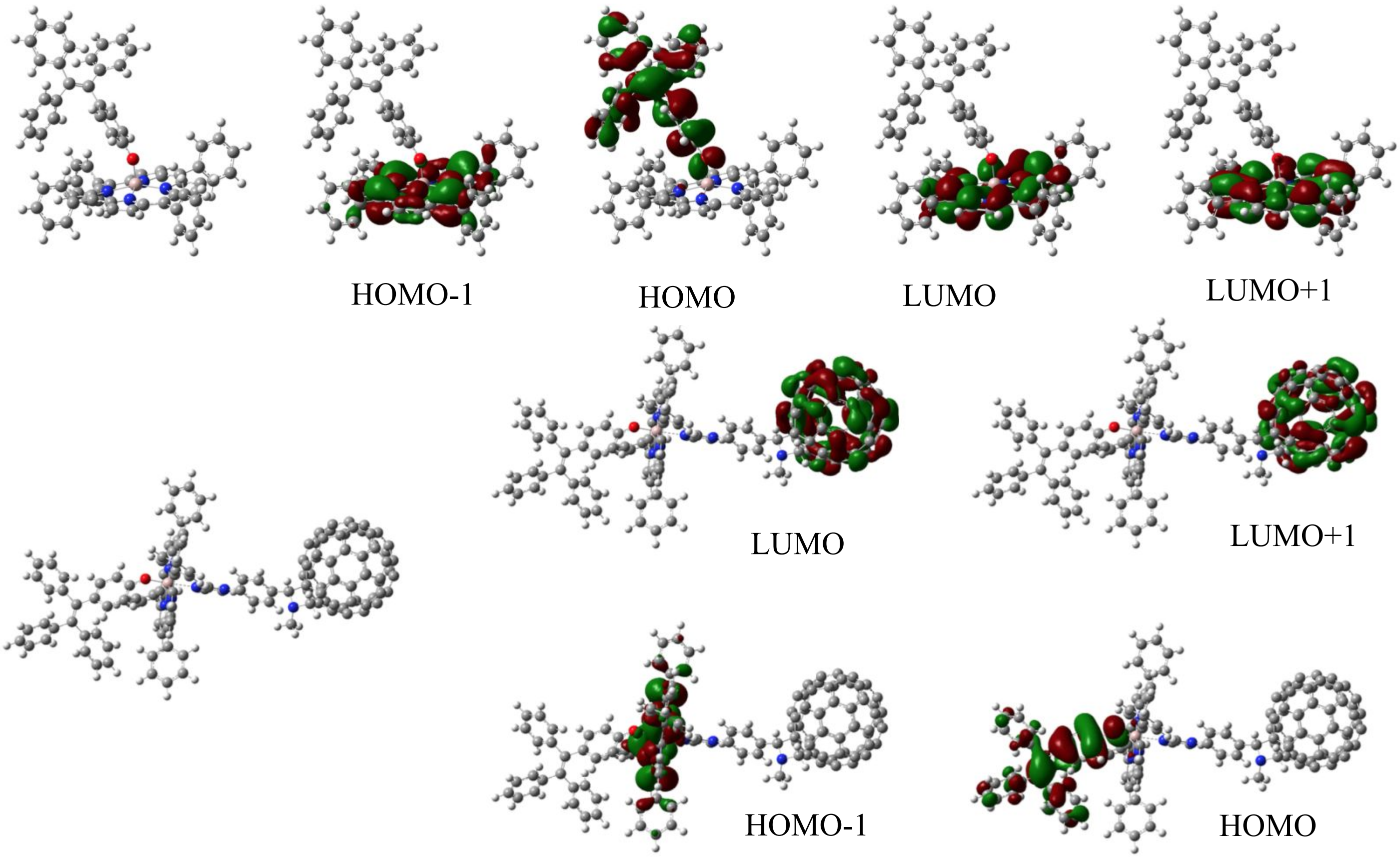

Figure 3. DFT calculated frontier orbitals of the dyad TPE-AlPor (top) and the triad TPE-AlPor←Im-C_{60} (bottom).

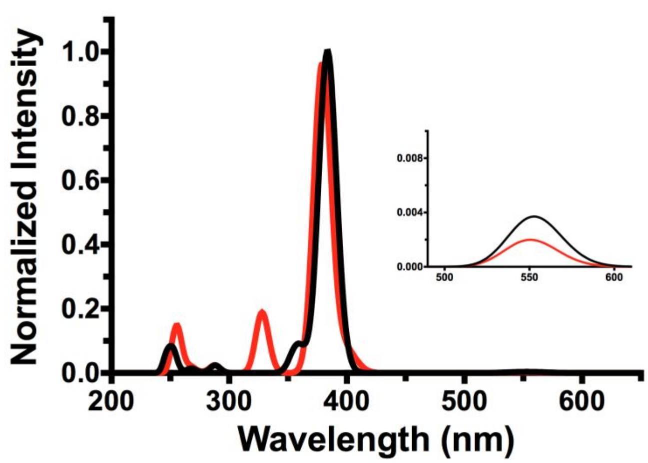

Figure 4. DFT calculated absorption profiles of TPE-AlPor (red) and AlPor-Ph (black).

Electrochemistry and Energetics. Redox potentials of the newly synthesized compounds were measured in 0.1 M TBA.ClO_4 dichloromethane with ferrocene as an internal standard. Representative voltammograms are shown in Figure 5, and the data is summarized in Table 1. The voltammogram of the dyad TPE-AlPor (Figure 5, bottom) is essentially a sum of the traces of the AlPor-Ph and TPE-OH references. Hence, the observed two reduction processes at −1.21 and −1.61 V are assigned to the first and second reduction of the AlPor unit. During the anodic scan two processes, at 0.93 and 1.17 V, were observed. Based on reference compounds the observed first oxidation is assigned to the first oxidation of AlPor, whereas, the second process is a combination of second oxidation of AlPor and first oxidation of TPE units. The redox processes of the AlPor are found to be one-electron reversible based on the peak-to-peak separation values, and the cathodic-to-anodic peak current ratio. However, the oxidation process of TPE could be irreversible or quasi-reversible. Furthermore, the observed processes are appeared without any perturbation in their redox potentials suggest the axial TPE/Ph unit do not influence significantly, due to weak coupling induced by the perpendicular orientation of the linker and porphyrin π-systems. The redox potentials of C_{60}-Im were adapted from the literature,[32] which showed three processes, −0.65, −1.03, −1.57, corresponding to its consecutive reductions of the C_{60} moiety.

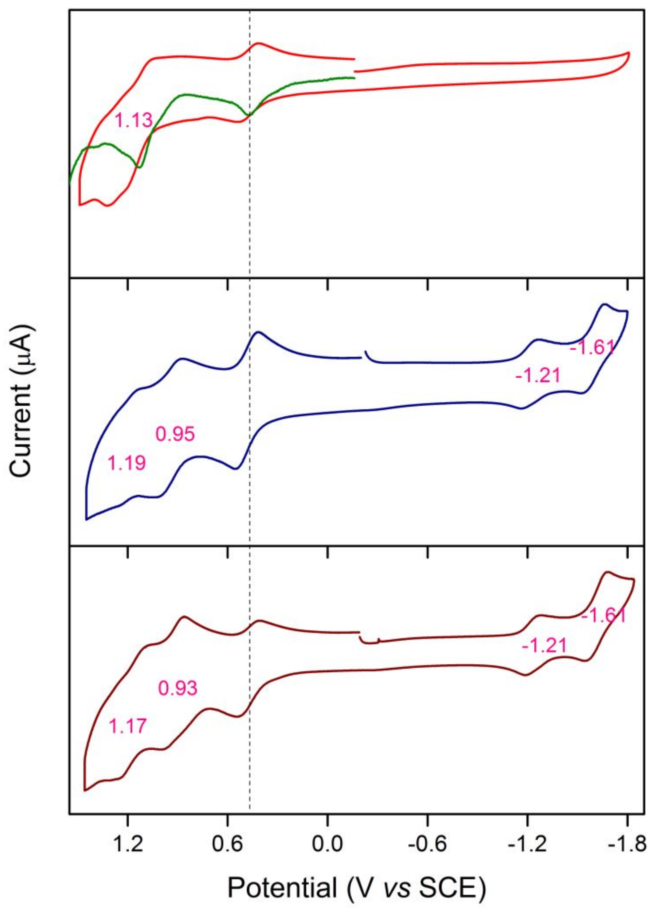

Figure 5. Cyclic voltammograms of TPE-OH (red) (green: differential voltammogram), AlPor-Ph (blue) and TPE-AlPor (maroon) with 0.1 M $TBA.ClO_4$ in dichloromethane. The experiments were measured with ferrocene (voltammogram at 0.48 *vs* SCE) as an internal standard. Scan rate 100 mV/s.

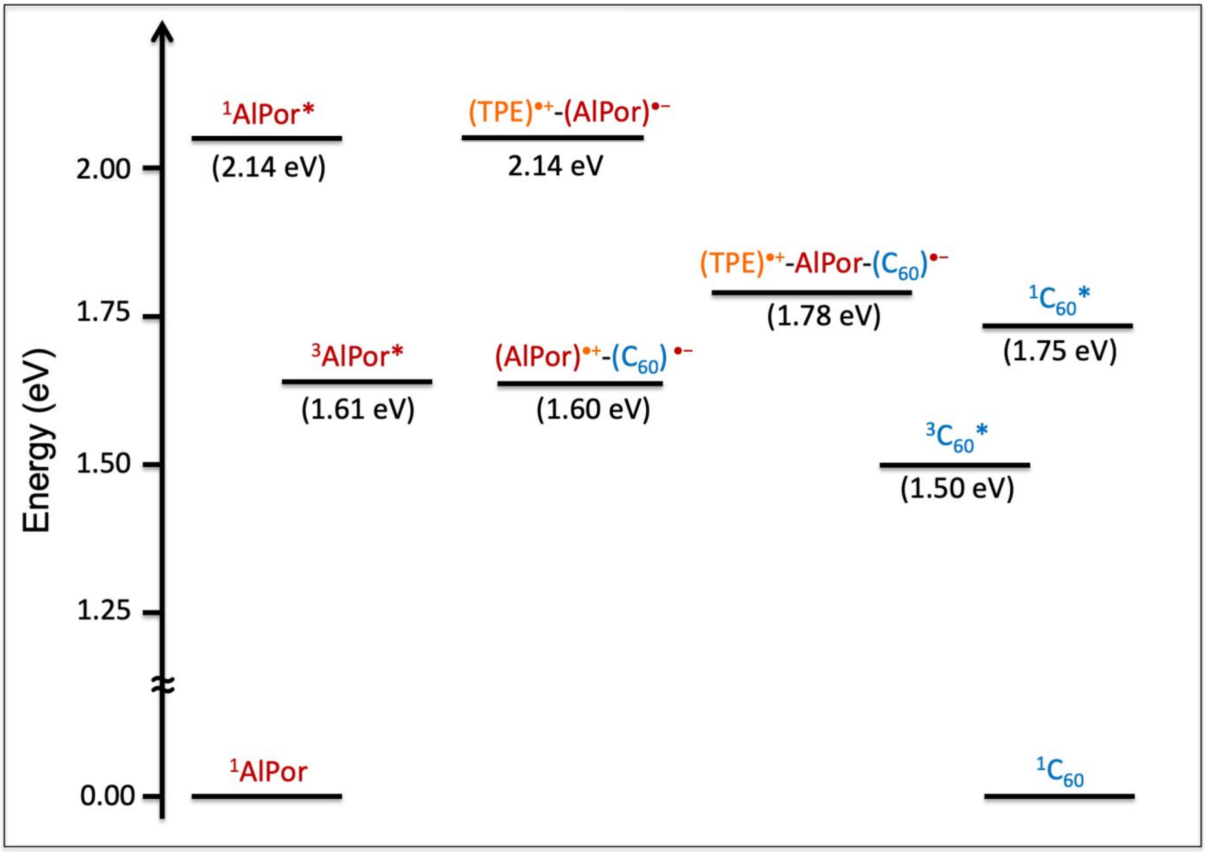

Figure 6. Energy level diagram of the photo- and redox-active units (AlPor, TPE, C_{60}) and possible charge separated states in toluene.

From the electrochemistry studies, it was revealed that the first oxidation of the TPE is overlapped with the second oxidation of the AlPor, therefore for the better estimation of the charge-separated state energy, we have used the reference TPE oxidation potential, 1.13 V, in our calculations. For the AlPor, potentials 0.95 V and –1.21 V are chosen as the first oxidation and first reduction processes, respectively. Whereas, the potential of –0.65 V was selected as the first reduction process for C_{60} moiety. The energy of the charge-separated states (E_{CS}) and the free-energy changes for charge separation (ΔG_{CS}) are given by Equations 1 and 2:[65-66]

$$E_{CS} = E^{ox}_{1/2}(Donor) - E^{red}_{1/2}(Acceptor) + G_S \qquad (1)$$

$$\Delta G_{CS} = E_{CS} - E_{0\text{-}0} \qquad (2)$$

where $E_{0\text{–}0}$ is the singlet-state energy of AlPor (2.14 eV).[47] G_S is the ion-pair stabilization and incorporates both the solvent-dependent Coulomb energy change upon ion-pair formation or recombination and the free energy of solvation of the ions, Equation 3:

$$G_S = e^2/(4\pi\varepsilon_0)[(1/(2R_+) + 1/(2R_-) - 1/R_{D\text{-}A})\ 1/\varepsilon_S - (1/(2R_+) + 1/(2R_-))\ 1/\varepsilon_R] \qquad (3)$$

where R_+, R_- and $R_{D\text{-}A}$ are donor radius, acceptor radius and the center-to-center distance between donor and acceptor, respectively. ε_S is the dielectric constant of solvent used for photophysical studies (8.9 and 2.4 for dichloromethane and toluene, respectively). ε_R is the dielectric constant of solvent used for measuring the redox potentials, in this case dichloromethane. By using the radii from the DFT calculations, G_S values of −0.22 and −0.20 eV for $TPE^{\bullet+}$-$AlPor^{\bullet-}$ in dichloromethane and toluene, respectively are obtained. It should be noted that the Coulomb term (G_S) was ignored for Ph-$(AlPor)^{\bullet+}$←Im-$(C_{60})^{\bullet-}$ and triad $(TPE)^{\bullet+}$-AlPor←Im-$(C_{60})^{\bullet-}$ species because of the relatively large $R_{D\text{-}A}$ values.[34-35] Using the energies obtained from the optical and electrochemical data, the energy-level diagram was constructed for the dyads and triads in dichloromethane (Figure S7) and toluene (Figure 6). It appears that the AlPor singlet excited and the $TPE^{\bullet+}$-$AlPor^{\bullet-}$ charge-separated states are very close in energy suggest that the photoinduced reductive electron transfer from TPE to $^1AlPor^*$ and followed by an electron shift to C_{60} are exergonic in dichloromethane and toluene solvents. On the other hand, the oxidative electron transfer from $^1AlPor^*$ to C_{60} is energetically favorable but the subsequent hole shift is uphill processes in both solvents.

Steady-state fluorescence studies. The steady-state fluorescence spectra of the TPE-AlPor and its reference compound AlPor-Ph were measured in toluene and dichloromethane. The experiments were carried out at the same concentration of porphyrin for all samples. The spectra were measured with an excitation wavelength of 550 nm, which excites the Q-band transition of the porphyrin. Figure 1b shows a comparison of the fluorescence spectra of TPE-AlPor with its reference compound AlPor-Ph. The spectral shapes and the emission maxima of the dyad are essentially the same as its reference compound AlPor-Ph. However, the fluorescence of the dyad is strongly quenched compared to that of the reference compound, which indicates the existence of a new relaxation process which is operating on the singlet excited state of porphyrin ($^1AlPor^*$) in presence of TPE entity. Singlet−singlet energy transfer can be safely ruled out as a quenching mechanism because the spectral overlap between AlPor emission and TPE absorption is essentially zero. On the other hand, the redox data (see Table 1) suggest that $TPE^{\bullet+}$-$AlPor^{\bullet-}$ is nearly isoenergetic with $^1AlPor^*$ in dichloromethane and toluene solvents. Hence, the observed quenching is more likely due to reductive electron transfer from TPE to $^1AlPor^*$.

To examine the influence of C_{60}-Im on the $^1AlPor^*$ state, the dyad TPE-AlPor was titrated with C_{60}-Im, see Figure 7a. The excitation wavelength was adjusted to the isosbestic point at 555 nm (see Figure 2a), which was obtained from absorption studies so that the extinction coefficient is the same for each sample solution. In the absence of C_{60}-Im, the fluorescence spectrum of the AlPor-Ph shows peaks at 595 and 645 nm. Upon addition of C_{60}-Im, a minor increase in the fluorescence followed by moderate quenching was noticed. The revealed spectral changes confirm the formation of the triad, TPE-AlPor←Im-C_{60}. However, to investigate the possible quenching mechanism several control experiments were carried out. When TPE-AlPor is titrated with Me-Im (lacking the C_{60}), primarily a redshift of the fluorescence bands with an increase in intensity (see Figure

S4c) was observed. The increase in intensity is due to changes in the intrinsic fluorescence rates as a result of structural modifications when imidazole coordinates to Al center. Whereas, titration of AlPor-Ph (lacking the TPE) with C_{60}-Im resulted in a strong quenching in AlPor fluorescence, see Figure 7b. Based on the energy level diagram, Figure 6, the observed strong quenching is attributed to the intramolecular oxidative electron transfer from ^{1}AlPor* to C_{60} entity to yield Ph-(AlPor)$^{•+}$←(C_{60})$^{•−}$, as the corresponding ΔG_{CS} for this process is estimated to be −0.54 eV. Therefore, the observed weak fluorescence quenching during the titration of TPE-AlPor *vs* C_{60}-Im is indeed due to an intramolecular oxidative electron transfer from ^{1}AlPor* to C_{60} moiety to yield TPE-(AlPor)$^{•+}$←Im-(C_{60})$^{•−}$. It is important to note that the fluorescence quenching is much weaker during the titration of TPE-AlPor *vs* C_{60}-Im than the AlPor-Ph *vs* C_{60}-Im suggest that the rate of the reductive electron transfer from TPE to ^{1}AlPor* could be faster than or at least similar with the oxidative electron transfer from ^{1}AlPor* to C_{60} entity. Under these conditions, it is reasonable to predict that the major part of the excited state ^{1}AlPor* in the triad TPE-AlPor←Im-C_{60} could be quenched by the reduction electron transfer from TPE to ^{1}AlPor* along with a minor oxidative electron transfer from ^{1}AlPor* to C_{60} unit. Hence, two charge-separated states (TPE)$^{•+}$-(AlPor)$^{•−}$←Im-C_{60} (major) and TPE-(AlPor)$^{•+}$←Im-(C_{60})$^{•−}$ (minor) are expected to be generated upon excitation of AlPor moiety in the triad. Based on the energy level diagram, the (TPE)$^{•+}$-(AlPor)$^{•−}$←Im-C_{60} state could further undergo a subsequent electron migration to produce (TPE)$^{•+}$-AlPor←Im-(C_{60})$^{•−}$ as a final charge-separated state. The free energy change for the electron migration (ΔG_{EM}) was found to be −0.34 eV and −0.36 eV in dichloromethane and toluene, respectively. Whereas, in the case of TPE-(AlPor)$^{•+}$←Im-(C_{60})$^{•−}$, the subsequent hole-shift, i.e. TPE-(AlPor)$^{•+}$←Im-(C_{60})$^{•−}$ to (TPE)$^{•+}$-AlPor←Im-(C_{60})$^{•−}$, is unlikely to take place because it is an uphill process, see Figures 6 and S7.

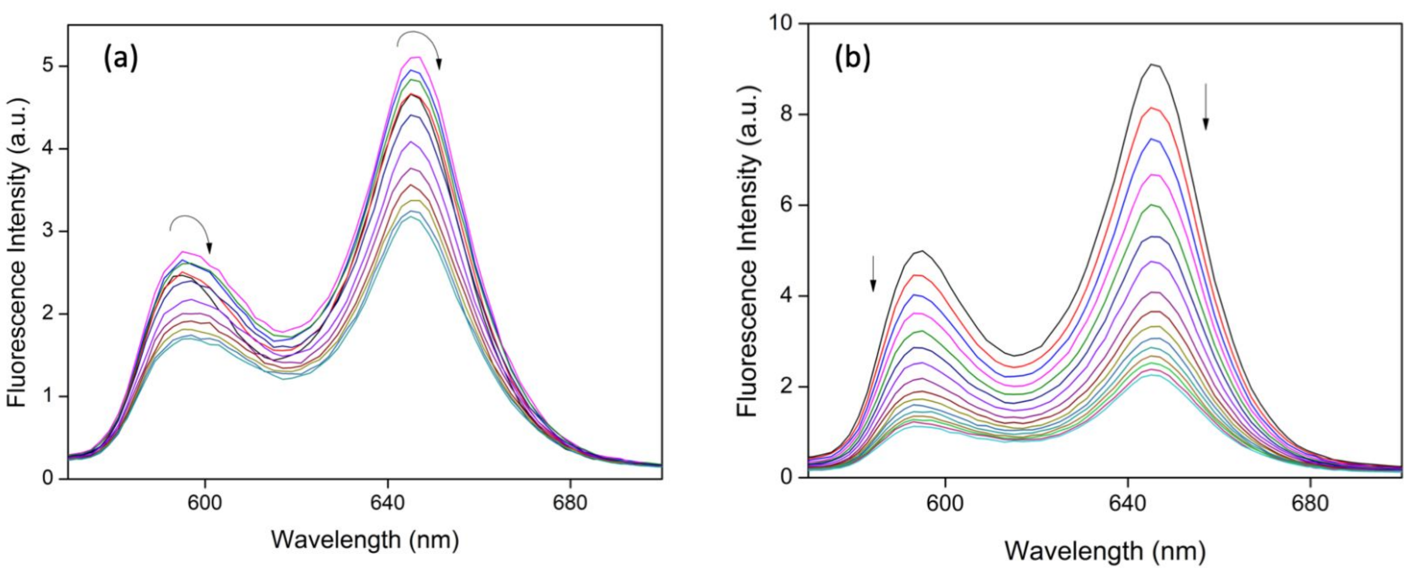

Figure 7. Fluorescence titrations of: (a) TPE-AlPor with C_{60}-Im, and (b) AlPor-Ph with C_{60}-Im. For the details of solution concentrations see Figure 2 caption. All titrations were performed in *o*-DCB, and the excitation

wavelength was chosen at the isosbestic point, 555 nm, which was obtained from corresponding absorption titrations.

Transient Absorption Spectroscopy. Femtosecond transient spectral studies were subsequently performed to probe the excited state events. Since, both DCM and *o*-DCB are not stable under strong laser irradiation, the transient absorption studies were performed in toluene. The transient spectra of the control compound AlPor-Ph, excited at 550 nm corresponding to visible peak maxima, is shown in Figure 8a. Immediately after excitation, a broad intense absorption increase with a maximum at 454 nm and additional peaks at 585 and 608 nm were observed. In addition to the absorption increase there were negative bands at 551 nm due to loss of the Q-band absorbance (ground state bleach) and at 600 and 652 nm due to emission from the S_1 state (stimulated emission). The absorbance increase and Q-band bleach were formed instantaneously as a result of the $S_0 \rightarrow S_n$ transition. The decay of these bands was beyond the 3 ns time window of our instrument in accordance with the 7.88 ns lifetime of the S_1 state determined by time correlated single photon counting (TCSPC) fluorescence measurements in toluene. There was a shoulder band at 490 nm and broad peak in the 800-900 nm range at late times, which we tentatively assigned to ^{3}AlPor*. Importantly, in the near-IR region, a peak at 1240 nm with the same decay profile as the singlet excited state is observed (see Figure 9c (i) for time profile), suggesting that this peak corresponds to excited singlet state absorption. Such near-IR peaks corresponding to singlet-singlet transition have also been reported for other porphyrin derivatives.[67]

The transient spectra of the dyad TPE-AlPor, excited at 550 nm, is shown in Figure 8b. In this case, the instantaneously formed ^{1}AlPor* had spectral characteristics similar to that of the control AlPor-Ph, however, the decay of the positive peaks and recovery of the negative peaks were rapid. These observations suggest the occurrence of excited state events, possibly generation of an energetically close charge separated state, TPE$^{\bullet+}$-AlPor$^{\bullet-}$ (See Figure 6 for energy level diagram). In such is the case, new transient peaks corresponding to AlPor$^{\bullet-}$ and TPE$^{\bullet+}$ could be expected. In order to characterize the one-electron reduced and one-electron oxidized products of AlPor, spectroelectrochemical studies were performed in *o*-DCB, as shown in Figure S8. During one-electron oxidation, new peaks at 600, 685, 791 and 882 nm, corresponding to AlPor$^{\bullet+}$, and during one-electron reduction new peaks at 570, 610 and 645 nm, corresponding to AlPor$^{\bullet-}$, were observed. It may be pointed out here that the intensity of the radical anions peaks were much smaller than that of the neutral species, making it difficult to spectrally isolate in the transient spectral data. Whereas, the counter cation, TPE$^{\bullet+}$, has a well-defined broad absorption features centered around 850 nm in near IR region,[68] and far enough to avoid overlap with porphyrin ground state and excited state transient features, therefore is an ideal for detection under transient experimental conditions. However, it may overlap with ^{3}AlPor* absorption features between 800-900 nm. Figure 9a shows the transient absorption spectrum of AlPor-Ph control and TPE-AlPor dyad at a delay time of 50 ps. As anticipated spectral features corresponding to AlPor$^{\bullet-}$ and TPE$^{\bullet+}$ are indeed observed in the range of

610 - 645 nm and 800-1000 nm (with contributions from ^{3}AlPor*), respectively providing proof for reductive electron transfer. The time profiles of the near-IR band corresponding to ^{1}AlPor* of the control and dyad are shown in Figure 9c, rapid decay of the dyad peak with a time constant of 234 ps was observed. The rate constant for charge separation, k_{CS} using this time constant and lifetime of ^{1}AlPor* was found to be 4.16 x 10^9 s^{-1}. Here it is important to note that the HOMO of the dyad TPE-AlPor extends onto the bridging phenoxy unit, bringing it into proximity of the LUMO and LUMO+1 which are localized on the AlPor entity. The resulting direct orbital overlap could help promote electron transfer even when the thermodynamic driving force is small, see Figure S9. This contrasts with the triad species, which has a large physical separation between the HOMO and HOMO-1 and the LUMO and LUMO+1, which are located on the C_{60} moiety, Figure 3. It is interesting to note that the formed charge-separated state holds high energy (E_{CS} = 2.14 eV), hence, it could relax to the ground state by populating the low-lying triplet state of ^{3}AlPor* = 1.61 eV or could relax directly to the ground state. More definite absorption feature between 800-900 nm was evidenced in the case of TPE-AlPor than the reference compound establishes relaxation of $TPE^{\bullet+}$-$AlPor^{\bullet-}$ state to triplet state of ^{3}AlPor*.

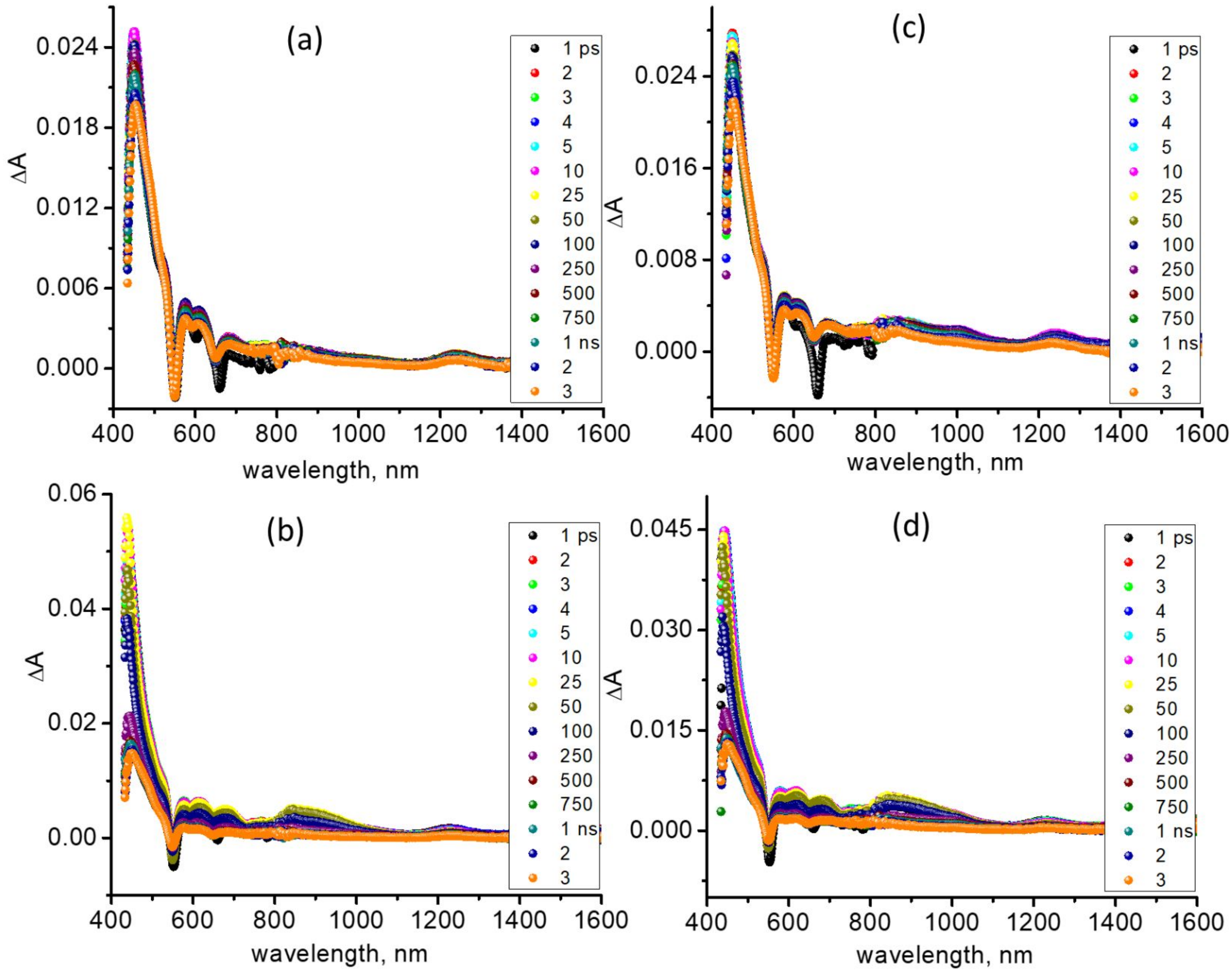

Figure 8. Femtosecond transient spectra at the indicated delay time of (a) AlPor-Ph, (b) TPE-AlPor, (c) Ph-AlPor←Im-C_{60}, and (d) TPE-AlPor←Im-C_{60} in toluene, excited at 550 nm.

Figure 8c shows the transient absorption spectra at different delay times of supramolecular Ph-AlPor←Im-C_{60} dyad, excited at 550 nm corresponding to AlPor. From the energy level diagram shown in Figure 6, charge separation from ^{1}AlPor* to generate Ph-AlPor$^{•+}$←Im-$(C_{60})^{•-}$ state is an energetically favourable process as the ΔG_{CS} for this process is estimated to be −0.54 eV. If such process occurs, one would expect rapid decay of the transient peaks originating from ^{1}AlPor* and new transient peaks corresponding to radical ion-pair species. Expectedly, the signature peak of $(C_{60})^{•-}$ at 1010 nm and a broad peak in the 880 nm range corresponding to AlPor$^{•+}$ which was overlapped with the ^{3}AlPor* in the spectral regions, were indeed observed thus providing evidence of charge separation in the dyad. Figure 9d shows the time profile of AlPor with and without coordinated C_{60}-Im. The decay profile of the Ph-AlPor←Im-C_{60} dyad was biexponential with a short-lived component of time constant of 616 ps and long-lived component with time constant beyond 3 ns. The short-lived component was attributed to the dyad undergoing charge separation and the long-lived component was attributed to unbound AlPor. The rate constant for charge separation, k_{CS} using this time constant and lifetime of ^{1}AlPor* was found to be 1.49 x 10^9 s^{-1}. In order to monitor the charge recombination, the decay of (C_{60}) peak at 1010 nm was monitored. As shown in Figure 9e(i), the delay lasted over 3 ns.

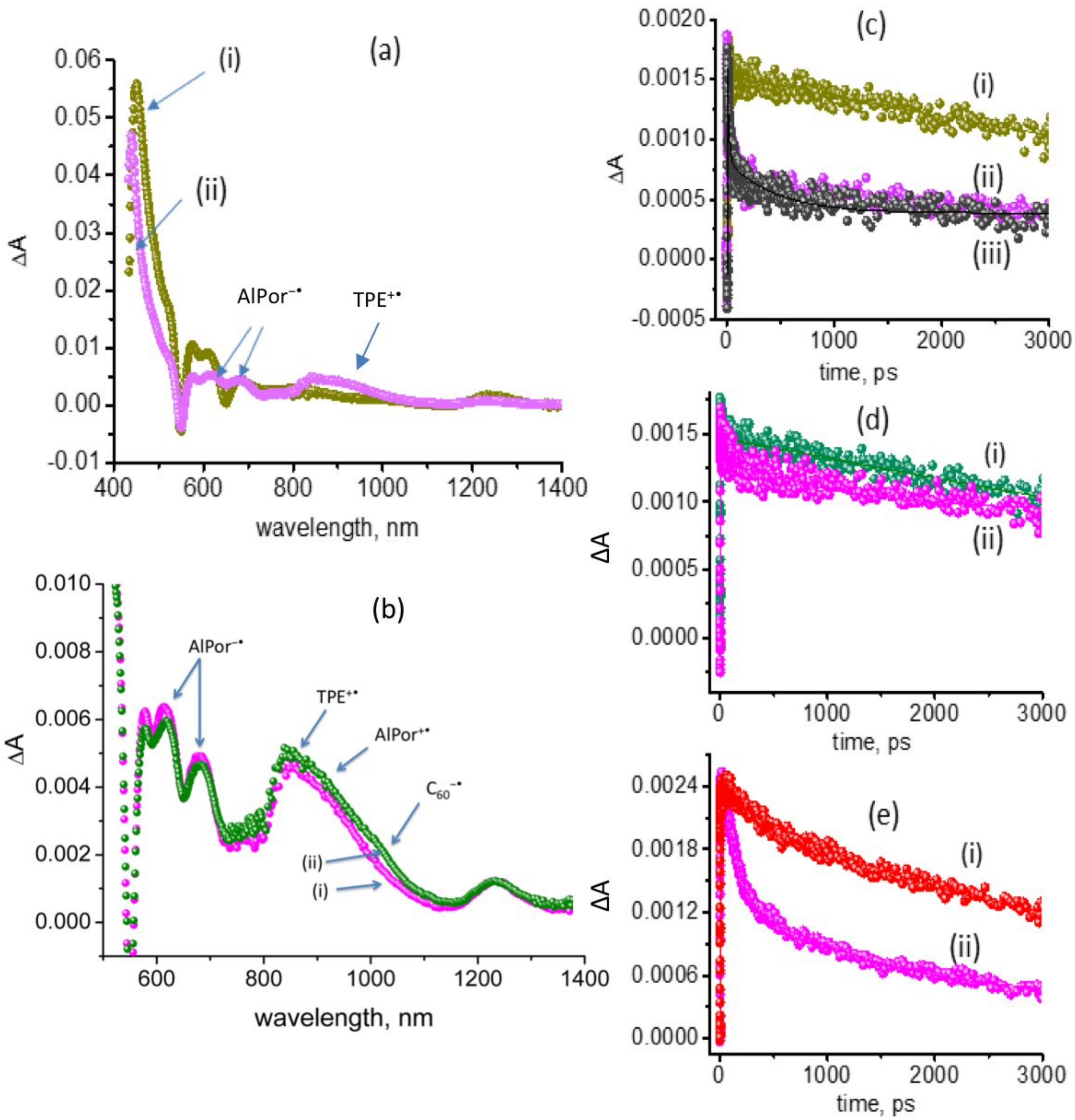

Figure 9. Femtosecond transient absorption spectra (a) at a delay time of 50 ps of (i) AlPor-Ph, and (ii) TPE-AlPor, and (b) at the delay time of 10 ps of (i) TPE-AlPor and (ii) TPE-AlPor←Im-C_{60} in toluene (λ_{ex} = 550 nm). Time profile of (c) the 1235 nm near-IR peak (i) AlPor-Ph, (ii) TPE-AlPor and (iii) TPE-AlPor←Im-C_{60} (d) the 1235 nm near-IR peak of (i) AlPor-Ph and (ii) Ph-AlPor←Im-C_{60} and (e) of the 1010 nm peak of (i) Ph-AlPor←Im-C_{60} and (ii) TPE-AlPor←Im-C_{60}.

Having established charge separation in the TPE-AlPor and Ph-AlPor←Im-C_{60} dyads, next we focused our attention to probe photochemical events in the TPE-AlPor←Im-C_{60} triad. There are at least two electron transfer paths originating from the ^{1}AlPor* in the triad, first, reductive electron transfer to yield $(TPE)^{\bullet+}$-$(AlPor)^{\bullet-}$←Im-C_{60} charge separated state and second, oxidative electron transfer to yield TPE-$(AlPor)^{\bullet+}$←Im-$(C_{60})^{\bullet-}$ charge separated state. Additionally, the former charge separated state could undergo an electron migration to coordinated C_{60} to yield $(TPE)^{\bullet+}$-AlPor←Im-$(C_{60})^{\bullet-}$ as the ultimate product. However, the later charge-separated state in unlikely to undergo hole shift as this is an uphill process. Due to distal separation of the positive and negative radical ions, a long-lived charge separated state could be envisioned. However, due to high energy stored in the $(TPE)^{\bullet+}$-AlPor←Im-$(C_{60})^{\bullet-}$ (E_{CS} = 1.78 eV), the charge separated state could relax to the ground state by populating one of the low-lying triplet states (^{3}AlPor* = 1.61 eV and $^{3}(C_{60})^{*}$ = 1.50 eV). Under such conditions, lifetime of $(TPE)^{\bullet+}$-AlPor←Im-$(C_{60})^{\bullet-}$ could be shortened considerably.

Figure 8d shows the transient absorption spectra of the TPE-AlPor←Im-C_{60} triad at different delay times, excited at 550 nm. The spectral features were indicative of charge separation in the triad. That is, transient peaks corresponding to both radical cation and radical anion were observed. This is shown in Figure 9b for the TPE-AlPor dyad and the TPE-AlPor←Im-C_{60} triad at a delay time of 10 ps. For the triad, the $(C_{60})^{\bullet-}$ peak at 1010 nm appeared as a shoulder peak to the broad peak in the 800-950 nm range what was completely missing in the case of the dyad. The decay of ^{1}AlPor* in the triad closely tracked that of the dyad TPE-AlPor (see Figure 9c(iii) for time profile). Assuming that it was mainly due to reductive electron transfer, the rate constant for charge separation, k_{CS} using this time constant and lifetime of ^{1}AlPor* was found to be 1.92×10^{9} s^{-1}, faster than that observed for Ph-AlPor←Im-C_{60}. The decay profiles of $(C_{60})^{\bullet-}$ for the TPE-AlPor←Im-C_{60} triad and Ph-AlPor←Im-C_{60} dyad, monitored at 1010 nm, are shown in Figure 9e. The persistence of $(C_{60})^{\bullet-}$ peak beyond 3 ns suggests an electron shift/hole transfer resulting into the formation of $(TPE)^{\bullet+}$-AlPor←Im-$(C_{60})^{\bullet-}$ charge separated state. Nanosecond transient absorption spectral studies did not reveal a signal corresponding to that of $(C_{60})^{\bullet-}$ indicating that the lifetime of final charge separated state is less than 25 ns, detection limit of our nanosecond transient setup. As pointed out earlier, the $(TPE)^{\bullet+}$-AlPor←Im-$(C_{60})^{\bullet-}$ state could relax to the ground state by populating either ^{3}AlPor* or $^{3}C_{60}$*, thus promoting the charge recombination process. In any event, although energetically not so favourable, we have been successful in observing charge separation in the TPE-AlPor dyad, that seem to also involve electron migration to result in the formation of $(TPE)^{\bullet+}$-AlPor←Im-$(C_{60})^{\bullet-}$ as an ultimate charge separated state.

Conclusions

The results presented above show that self-assembled triad capable of step-wise, light-induced charge separation can be constructed by coordinating imidazole-appended C_{60} derivative with the TPE-AlPor dyad. One of the key differences between our previously reported self-assembled triads[46-48, 50-51] and the present triad is the nature of the linkage between AlPor and its redox counterparts (i.e., the electron donor and acceptor units). In earlier reported triads, the electron acceptor was covalently linked to the central AlPor, whereas the secondary electron donor was linked through coordination bond by using either pyridine or imidazole moiety. In the present triad, it was quite opposite where the electron donor and acceptor were linked through covalent and coordination bonds, respectively. The steady state and transient absorption studies reveals the initial charge separation occurs between TPE and AlPor to produce $(TPE)^{\bullet+}$-$(AlPor)^{\bullet-}$←Im-C_{60} state, which subsequently undergo charge shift to C_{60} to generate $(TPE)^{\bullet+}$-AlPor←Im-$(C_{60})^{\bullet-}$ radical pair as an ultimate state with a lifetime of 25 ns. Remarkably, the observed charge-separated states hold high energies, 2.14 and 1.78 eV for $(TPE)^{\bullet+}$-$(AlPor)^{\bullet-}$←Im-C_{60} and $(TPE)^{\bullet+}$-AlPor←Im-$(C_{60})^{\bullet-}$, respectively. Therefore, the studied dyad and triad could be potential candidates in the areas of artificial photosynthesis for producing energy demanding light-to-fuel products. Studies are in progress to improve the lifetimes of the investigated donor-acceptor systems.

Supporting Information Available: Details of ESI mass spectrum, NMR spectra, absorption, and fluorescence titrations, natural transition orbital analysis, energy level diagram, and spectroelectrochemistry.

Acknowledgements

This work was supported by the University of Minnesota Duluth (startup funds) to PPK, and by the National Science Foundation (Grant No. 1401188) to FD. V.S.B. acknowledges support by LEAP, an Energy Frontier Research Center funded by the U.S. DOE under Award No. DE-SC0001059 and DOE supercomputer time from NERSC. CA thanks the Natural Sciences and Engineering Research Council of Canada for a postdoctoral fellowship.

References and Notes

1. Armaroli, N.; Balzani, V., The Future of Energy Supply: Challenges and Opportunities. *Angew. Chem.-Int. Edit.* **2007**, *46*, 52-66.
2. Armaroli, N.; Balzani, V., Solar Electricity and Solar Fuels: Status and Perspectives in the Context of the Energy Transition. *Chemistry-a European Journal* **2016**, *22*, 32-57.
3. Barber, J., Photosynthetic Energy Conversion: Natural and Artificial. *Chem. Soc. Rev.* **2009**, *38*, 185-196.
4. Hambourger, M.; Moore, G. F.; Kramer, D. M.; Gust, D.; Moore, A. L.; Moore, T. A., Biology and Technology for Photochemical Fuel Production. *Chem. Soc. Rev.* **2009**, *38*, 25-35.
5. El-Khouly, M. E.; El-Mohsnawy, E.; Fukuzumi, S., Solar Energy Conversion: From Natural to Artificial Photosynthesis. *J. Photochem. Photobiol. C-Photochem. Rev.* **2017**, *31*, 36-83.
6. Gust, D., An Illustrative History of Artificial Photosynthesis. In *Artificial Photosynthesis*, Bruno, R., Ed. 2016; Vol. 79, pp 1-42.
7. Fukuzumi, S.; Ohkubo, K.; Suenobu, T., Long-Lived Charge Separation and Applications in Artificial Photosynthesis. *Acc Chem. Res.* **2014**, *47*, 1455-1464.
8. Kalyanasundaram, K.; Graetzel, M., Artificial Photosynthesis: Biomimetic Approaches to Solar Energy Conversion and Storage. *Current Opinion in Biotechnology* **2010**, *21*, 298-310.

9. Gust, D.; Moore, T. A.; Moore, A. L., Solar Fuels Via Artificial Photosynthesis. *Acc Chem. Res.* **2009**, *42*, 1890-1898.
10. Alstrum-Acevedo, J. H.; Brennaman, M. K.; Meyer, T. J., Chemical Approaches to Artificial Photosynthesis. 2. *Inorganic Chemistry* **2005**, *44*, 6802-6827.
11. Deisenhofer, J.; Epp, O.; Miki, K.; Huber, R.; Michel, H., X-Ray Structure-Analysis of a Membrane-Protein Complex - Electron-Density Map at 3a Resolution and a Model of the Chromophores of the Photosynthetic Reaction Center from Rhodopseudomonas-Viridis. *J. Mol. Biol.* **1984**, *180*, 385-398.
12. Fromme, P., Structure and Function of Photosystem I. *Curr. Opin. Struct. Biol.* **1996**, *6*, 473-484.
13. Krauss, N.; Schubert, W. D.; Klukas, O.; Fromme, P.; Witt, H. T.; Saenger, W., Photosystem I at 4 Angstrom Resolution Represents the First Structural Model of a Joint Photosynthetic Reaction Centre and Core Antenna, System. *Nat. Struct. Biol.* **1996**, *3*, 965-973.
14. Bottari, G.; Trukhina, O.; Ince, M.; Torres, T., Towards Artificial Photosynthesis: Supramolecular, Donor-Acceptor, Porphyrin-and Phthalocyanine/Carbon Nanostructure Ensembles. *Coord. Chem. Rev.* **2012**, *256*, 2453-2477.
15. Harriman, A.; Sauvage, J. P., Strategy for Constructing Photosynthetic Models: Porphyrin-Containing Modules Assembled around Transition Metals. *Chem. Soc. Rev.* **1996**, *25*, 41-&.
16. Gould, S. L.; Kodis, G.; Palacios, R. E.; de la Garza, L.; Brune, A.; Gust, D.; Moore, T. A.; Moore, A. L., Artiflcial Photosynthetic Reaction Centers with Porphyrins as Primary Electron Acceptors. *J. Phys. Chem. B* **2004**, *108*, 10566-10580.
17. Boyd, P. D. W.; Reed, C. A., Fullerene-Porphyrin Constructs. *Acc Chem. Res.* **2005**, *38*, 235-242.
18. Wasielewski, M. R., Self-Assembly Strategies for Integrating Light Harvesting and Charge Separation in Artificial Photosynthetic Systems. *Acc Chem. Res.* **2009**, *42*, 1910-1921.
19. D'Souza, F.; Gadde, S.; Islam, D. M. S.; Wijesinghe, C. A.; Schumacher, A. L.; Zandler, M. E.; Araki, Y.; Ito, O., Multi-Triphenylamine-Substituted Porphyrin-Fullerene Conjugates as Charge Stabilizing "Antenna-Reaction Center" Mimics. *Journal of Physical Chemistry A* **2007**, *111*, 8552-8560.
20. Aratani, N.; Kim, D.; Osuka, A., Discrete Cyclic Porphyrin Arrays as Artificial Light-Harvesting Antenna. *Acc Chem. Res.* **2009**, *42*, 1922-1934.
21. Fukuzumi, S., Development of Bioinspired Artificial Photosynthetic Systems. *Phys. Chem. Chem. Phys.* **2008**, *10*, 2283-2297.
22. Guldi, D. M., Fullerene-Porphyrin Architectures; Photosynthetic Antenna and Reaction Center Models. *Chem. Soc. Rev.* **2002**, *31*, 22-36.
23. Gust, D.; Moore, T. A., Photosynthetic Model Systems. *Top Curr Chem* **1991**, *159*, 103-151.
24. Gust, D.; Moore, T. A.; Moore, A. L., Mimicking Photosynthetic Solar Energy Transduction. *Acc Chem. Res.* **2001**, *34*, 40-48.
25. Imahori, H., Porphyrin-Fullerene Linked Systems as Artificial Photosynthetic Mimics. *Organic & Biomolecular Chemistry* **2004**, *2*, 1425-1433.
26. Imahori, H.; Mori, Y.; Matano, Y., Nanostructured Artificial Photosynthesis. *J. Photochem. Photobiol. C-Photochem. Rev.* **2003**, *4*, 51-83.
27. Kamat, P. V., Meeting the Clean Energy Demand: Nanostructure Architectures for Solar Energy Conversion. *Journal of Physical Chemistry C* **2007**, *111*, 2834-2860.
28. Liu, J. Y.; El-Khouly, M. E.; Fukuzumi, S.; Ng, D. K. P., Mimicking Photosynthetic Antenna-Reaction-Center Complexes with a (Boron Dipyrromethene)(3)-Porphyrin-C60 Pentad. *Chemistry-a European Journal* **2011**, *17*, 1605-1613.
29. Schmittel, M.; Kishore, R. S. K.; Bats, J. W., Synthesis of Supramolecular Fullerene-Porphyrin-Cu(Phen)(2)-Ferrocene Architectures. A Heteroleptic Approach Towards Tetrads. *Organic & Biomolecular Chemistry* **2007**, *5*, 78-86.
30. D'Souza, F.; El-Khouly, M. E.; Gadde, S.; Zandler, M. E.; McCarty, A. L.; Araki, Y.; Ito, O., Supramolecular Triads Bearing Porphyrin and Fullerene Via 'Two-Point' Binding Involving Coordination and Hydrogen Bonding. *Tetrahedron* **2006**, *62*, 1967-1978.

31. El-Khouly, M. E.; Gadde, S.; Deviprasad, G. R.; Fujitsuka, M.; Ito, O.; D'Souza, F., Self-Assembled Supramolecular Triad Composed of Fulleropyrrolidine Bearing Two Pyridine Moieties Axially Coordinated to Two Zinc Porphyrins. *J. Porphyrins and Phthalocyanines* **2003**, *7*, 1-7.
32. D'Souza, F.; Smith, P. M.; Zandler, M. E.; McCarty, A. L.; Itou, M.; Araki, Y.; Ito, O., Energy Transfer Followed by Electron Transfer in a Supramolecular Triad Composed of Boron Dipyrrin, Zinc Porphyrin, and Fullerene: A Model for the Photosynthetic Antenna-Reaction Center Complex. *J. Am. Chem. Soc.* **2004**, *126*, 7898-7907.
33. Favereau, L.; Makhal, A.; Pellegrin, Y.; Blart, E.; Petersson, J.; Goransson, E.; Hammarstrom, L.; Odobel, F., A Molecular Tetrad That Generates a High-Energy Charge-Separated State by Mimicking the Photosynthetic Z-Scheme. *J. Am. Chem. Soc.* **2016**, *138*, 3752-3760.
34. Imahori, H.; Tamaki, K.; Guldi, D. M.; Luo, C. P.; Fujitsuka, M.; Ito, O.; Sakata, Y.; Fukuzumi, S., Modulating Charge Separation and Charge Recombination Dynamics in Porphyrin Fullerene Linked Dyads and Triads: Marcus-Normal Versus Inverted Region. *J. Am. Chem. Soc.* **2001**, *123*, 2607-2617.
35. Luo, C.; Guldi, D. M.; Imahori, H.; Tamaki, K.; Sakata, K., Sequential Energy and Electron Transfer in an Artificial Reaction Center: Formation of a Long-Lived Charge-Separated State. *J. Am. Chem. Soc.* **2000**, *122*, 6535-6551.
36. Das, S. K.; Mahler, A.; Wilson, A. K.; D'Souza, F., High-Potential Perfluorinated Phthalocyanine-Fullerene Dyads for Generation of High-Energy Charge-Separated States: Formation and Photoinduced Electron-Transfer Studies. *Chemphyschem* **2014**, *15*, 2462-2472.
37. Lim, G. N.; Obondi, C. O.; D'Souza, F., A High-Energy Charge-Separated State of 1.70ev from a High-Potential Donor-Acceptor Dyad: A Catalyst for Energy-Demanding Photochemical Reactions. *Angew. Chem.-Int. Edit.* **2016**, *55*, 11517-11521.
38. Cantu, R.; Seetharaman, S.; Babin, E. M.; Karr, P. A.; D'Souza, F., Paddle-Wheel Bodipy-Hexaoxatriphenylene Conjugates: Participation of Redox-Active Hexaoxatriphenylene in Excited-State Charge Separation to Yield High-Energy Charge-Separated States. *Journal of Physical Chemistry A* **2018**, *122*, 3780-3786.
39. Poddutoori, P. K.; Poddutoori, P.; Maiya, B. G.; Prasad, T. K.; Kandrashkin, Y. E.; Vasil'ev, S.; Bruce, D.; van der Est, A., Redox Control of Photoinduced Electron Transfer in Axial Terpyridoxy Porphyrin Complexes. *Inorganic Chemistry* **2008**, *47*, 7512-7522.
40. Bagaki, A.; Gobeze, H. B.; Charalambidis, G.; Charisiadis, A.; Stangel, C.; Nikolaou, V.; Stergiou, A.; Tagmatarchis, N.; D'Souza, F.; Coutsolelos, A. G., Axially Assembled Photosynthetic Antenna-Reaction Center Mimics Composed of Boron Dipyrromethenes, Aluminum Porphyrin, and Fullerene Derivatives. *Inorganic Chemistry* **2017**, *56*, 10268-10280.
41. Amati, A.; Cavigli, P.; Kahnt, A.; Indelli, M. T.; Iengo, E., Self-Assembled Ruthenium(Ii)Porphyrin-Aluminium(Iii)Porphyrin-Fullerene Triad for Long-Lived Photoinduced Charge Separation. *Journal of Physical Chemistry A* **2017**, *121*, 4242-4252.
42. Davidson, G. J. E.; Tong, L. H.; Raithby, P. R.; Sanders, J. K. M., Aluminium(Iii) Porphyrins as Supramolecular Building Blocks. *Chem. Commun.* **2006**, 3087-3089.
43. Iengo, E.; Cavigli, P.; Gamberoni, M.; Indelli, M. T., A Selective Metal-Mediated Approach for the Efficient Self-Assembling of Multi-Component Photoactive Systems. *Eur. J. Inorg. Chem.* **2014**, *2014*, 337-344.
44. Iengo, E.; Pantos, G. D.; Sanders, J. K. M.; Orlandi, M.; Chiorboli, C.; Fracasso, S.; Scandola, F., A Fully Self-Assembled Non-Symmetric Triad for Photoinduced Charge Separation. *Chemical Science* **2011**, *2*, 676-685.
45. Metselaar, G. A.; Sanders, J. K. M.; de Mendoza, J., A Self-Assembled Aluminium(Iii) Porphyrin Cyclic Trimer. *Dalton Trans.* **2008**, 588-590.
46. Poddutoori, P. K.; Bregles, L. P.; Lim, G. N.; Boland, P.; Kerr, R. G.; D'Souza, F., Modulation of Energy Transfer into Sequential Electron Transfer Upon Axial Coordination of Tetrathiafulvalene in an Aluminum(Iii) Porphyrin-Free-Base Porphyrin Dyad. *Inorganic Chemistry* **2015**, *54*, 8482-8494.

47. Poddutoori, P. K.; Lim, G. N.; Sandanayaka, A. S. D.; Karr, P. A.; Ito, O.; D'Souza, F.; Pilkington, M.; van der Est, A., Axially Assembled Photosynthetic Reaction Center Mimics Composed of Tetrathiafulvalene, Aluminum(Iii) Porphyrin and Fullerene Entities. *Nanoscale* **2015**, *7*, 12151-12165.
48. Poddutoori, P. K.; Lim, G. N.; Vassiliev, S.; D'Souza, F., Ultrafast Charge Separation and Charge Stabilization in Axially Linked Letrathiafulvalene-Aluminum(Iii) Porphyrin-Gold(Iii) Porphyrin' Reaction Center Mimics. *Phys. Chem. Chem. Phys.* **2015**, *17*, 26346-26358.
49. Poddutoori, P. K.; Sandanayaka, A. S. D.; Hasobe, T.; Ito, O.; van der Est, A., Photoinduced Charge Separation in a Ferrocene-Aluminum(Iii) Porphyrin-Fullerene Supramolecular Triad. *J. Phys. Chem. B* **2010**, *114*, 14348-14357.
50. Poddutoori, P. K.; Sandanayaka, A. S. D.; Zarrabi, N.; Hasobe, T.; Ito, O.; van der Est, A., Sequential Charge Separation in Two Axially Linked Phenothiazine-Aluminum(Iii) Porphyrin-Fullerene Triads. *Journal of Physical Chemistry A* **2011**, *115*, 709-717.
51. Poddutoori, P. K.; Zarrabi, N.; Moiseev, A. G.; Gumbau-Brisa, R.; Vassiliev, S.; van der Est, A., Long-Lived Charge Separation in Novel Axial Donorporphyrinacceptor Triads Based on Tetrathiafulvalene, Aluminum(Iii) Porphyrin and Naphthalenediimide. *Chemistry-a European Journal* **2013**, *19*, 3148-3161.
52. Guldi, D.; Martin, N., *Electron Transfer in Functionalized Fullerenes. In Fullerenes: From Synthesis to Optoelectronic Properties* Kluwer Academic Publishers: Norwell, MA, 2002; p 163-212.
53. Guldi, D. M., Fullerenes: Three Dimensional Electron Acceptor Materials. *Chem. Commun.* **2000**, 321-327.
54. Nalwa, H. S., *Photochemistry of Fullernes. In Handbook of Photochemistry and Photobiology, Vol. 2; Organic Photochemistry*. 2003; p 111-145.
55. Abd-El-Aziz, A. S.; Agatemor, C.; Etkin, N.; Wagner, B., Photoinduced Synthesis of Dual-Emissive Tetraphenylethene-Based Dendrimers with Tunable Aggregates and Solution States Emissions. *Macromol. Rapid Commun.* **2016**, *37*, 1235-1241.
56. Benesi, H. A.; Hildebrand, J. H., A Spectrophotometric Investigation of the Interaction of Iodine with Aromatic Hydrocarbons. *J. Am. Chem. Soc.* **1949**, *71*, 2703-2707.
57. Becke, A. D., Density-Functional Thermochemistry .3. The Role of Exact Exchange. *Journal of Chemical Physics* **1993**, *98*, 5648-5652.
58. Weigend, F.; Ahlrichs, R., Balanced Basis Sets of Split Valence, Triple Zeta Valence and Quadruple Zeta Valence Quality for H to Rn: Design and Assessment of Accuracy. *Phys. Chem. Chem. Phys.* **2005**, *7*, 3297-3305.
59. Marenich, A. V.; Cramer, C. J.; Truhlar, D. G., Universal Solvation Model Based on Solute Electron Density and on a Continuum Model of the Solvent Defined by the Bulk Dielectric Constant and Atomic Surface Tensions. *J. Phys. Chem. B* **2009**, *113*, 6378-6396.
60. Konezny, S. J.; Doherty, M. D.; Luca, O. R.; Crabtree, R. H.; Soloveichik, G. L.; Batista, V. S., Reduction of Systematic Uncertainty in Dft Redox Potentials of Transition-Metal Complexes. *Journal of Physical Chemistry C* **2012**, *116*, 6349-6356.
61. Furche, F.; Ahlrichs, R., Adiabatic Time-Dependent Density Functional Methods for Excited State Properties. *Journal of Chemical Physics* **2002**, *117*, 7433-7447.
62. Yanai, T.; Tew, D. P.; Handy, N. C., A New Hybrid Exchange-Correlation Functional Using the Coulomb-Attenuating Method (Cam-B3lyp). *Chemical Physics Letters* **2004**, *393*, 51-57.
63. Frisch, M. J., et al., *Gaussian 09* Gaussian Inc. Wallingford CT 2009, 2009.
64. Martin, R. L., Natural Transition Orbitals. *Journal of Chemical Physics* **2003**, *118*, 4775-4777.
65. Rehm, D.; Weller, A., Kinetics and Mechanics of Electron Transfer During Fluorescence Quenching in Acetonitrile. *Berichte Der Bunsen-Gesellschaft Fur Physikalische Chemie* **1969**, *73*, 834-839.
66. Rehm, D.; Weller, A., Kinetics of Fluorescence Quenching by Electron and H-Atom Transfer. *Israel Journal of Chemistry* **1970**, *8*, 259-&.
67. Schalk, O.; Brands, H.; Balaban, T. S.; Unterreiner, A.-N., Near-Infrared Excitation of the Q Band in Free Base and Zinc Tetratolyl-Porphyrins. *Journal of Physical Chemistry A* **2008**, *112*, 1719-1729.

68. Vyas, V. S.; Rathore, R., Preparation of a Tetraphenylethylene-Based Emitter: Synthesis, Structure and Optoelectronic Properties of Tetrakis(Pentaphenylphenyl)Ethylene. *Chem. Commun.* **2010**, *46*, 1065-1067.

TOC Graphic:

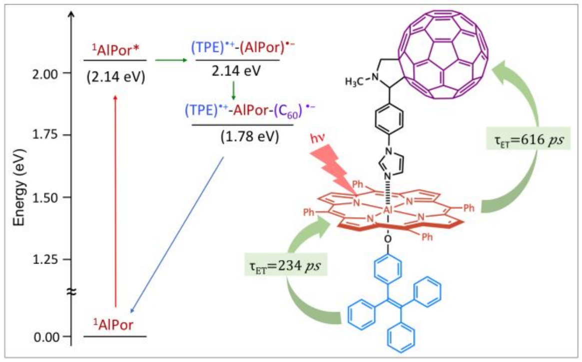

Energy (eV)
2.00
1.75
1.50
1.25
0.00
^{1}AlPor*
(2.14 eV)
(TPE)$^{\bullet+}$-(AlPor)$^{\bullet-}$
2.14 eV
(TPE)$^{\bullet+}$-AlPor-(C$_{60}$)$^{\bullet-}$
(1.78 eV)
^{1}AlPor
hν
τ_{ET}=616 ps
τ_{ET}=234 ps